16th ICAAR LISBOA 2020-2022

16th International Conference on
Alkali-Aggregate Reaction in Concrete
Lisboa | LNEC | Portugal | 31 May - 2 June 2022

http://icaar2020-2022.lnec.pt

Stirrup ruptures through experimental and analytical simulations

Kenji Kosa [(1)], Yulong Zheng [(2)], Nobuo Uehara [(3)]

(1) Kyushu Institute of Technology, Kitakyushu, Japan, kosakenji@yahoo.co.jp

(2) Jiangsu University, Jiangsu, China, zylpuff@yahoo.co.jp

(3) Sumitomo Osaka Cement, Kanazawa, Japan, nuehara@soc.co.jp

Abstract

To estimate the behavior of stirrups, which is necessary for understanding the reason for stirrups rupturing due to Alkali-Silica Reaction (ASR), experiments simulating ASR expansion were conducted. First, an instance of rupture of steel reinforcements is presented. Second, using 1/4 scale of the actual structure with old type stirrups, specimens were made by casting expansive mortar into the square hollow of ordinary concrete set to provide adhesion for the stirrups. The results showed that corresponding to external cracking caused by bending and tensile effects, ASR-induced uniform elongation and circumferential deformation were generated. This was confirmed to induce the progress of crack initiations in stirrups and even ruptures.

***Keywords**: ASR; experiment; circumferential deformation; stirrup rupture*

1. DAMAGED STRUCTURES DUE TO ASR IN JAPAN

In recent years, due to Alkali-Silica Reaction (ASR), many concrete structures have been affected by significant deterioration. For example, according to Torii [1], a large number of about 40 structures in Japan was detected to have rupture of steel reinforcements due to excessive expansion from ASR.

Figure 1.1 presents the ASR-affecting areas (gray areas) and regions (indicated by circles) with rupture of steel reinforcements discovered in Japan. It can be inferred from Figure 1.1 that the impact by ASR is not a problem occurred in the limited area but in all of the Japan.

As an instance of rupture of steel reinforcements, Figure 1.2 presents one pier taken from the bridge built at 1972 and located in the Hokuriku Region of Japan. The ASR deterioration becomes obvious in this bridge after 17 years of services. During 5 years after the maintenance of surface coating, cracking appeared again on the surface coating materials, which indicates the great deteriorative degree. Herein, the rupture conditions are stated. Figure 1.3(a) illustrates the reinforcements of the cross section. The bent part of stirrup is named like TU, KU, KL and TL for the following descriptions. Three damage types are defined based on the visual observations. As shown in Figure 1.3(b) (viewed from the right side, refer to Figure 1.2), along with the beam axis, many reinforcements are confirmed to be damaged (reinforcements ruptured or with crack initiation progressed). There are reinforcements damaged continuously as illustrated in area (1) of Figure 1.3; while there are also reinforcements damaged individually as in area (2) of Figure 1.3.

Figure 1.4 shows the percentage of the damaged reinforcements in total reinforcements. As for the damage ratio (ratio of number for damaged reinforcements to the total number), 69%, 46%, 25% and 20% is counted for the KU, TU, KL and TL side, respectively. The upper side of beam was found to have greater damage ratio relatively. In general, the total damage ratio of this pier is around 46%, from which, great deterioration is confirmed to occur. Figure 1.5 illustrates the cracking conditions in the right profile. The data was recorded on the surface coating material. The general cracking density in profile is 3.38m/m^2 and the maximum cracking width is around 2.0mm. In the general profile, it is observed that cracks are notable in horizontal direction. Though after the surface coating, cracking with width greater than 1.0mm generated. The notable cracking in horizontal direction is located in around 1500 mm below the upper surface. Further, as the maximum thickness of covering layer for stirrup is confirmed to be about 300mm, it is estimated that the bent part of stirrup has over 1000 mm height difference with the notable horizontal cracking. Thus, based on Uehara [2], it considered to be difficult to conclude that the occurrence of great cracking is correlated with the damage of reinforcement.

As an overview of cracks inside the beam, Figure 1.6 shows the cracks on the cross section of the beam. With regard to cracks inside RC members, it was considered that there was no significant damage when

appropriate reinforcing reinforcement restraint was applied. However, it was confirmed that the crack density of the cross section for cracks with a width of 0.2 mm or more was 6.13 m / m^2.

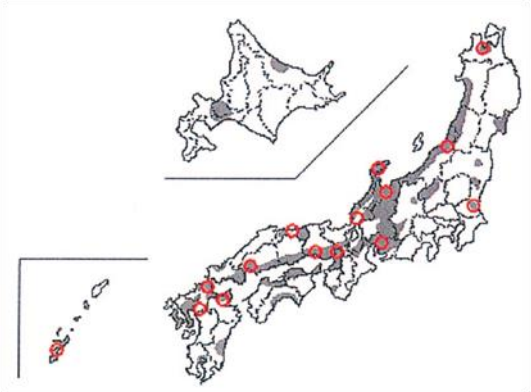

Figure 1.1: ASR-affecting area in Japan

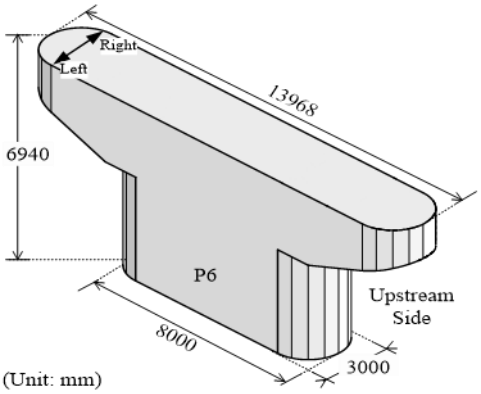

Figure 1.2: Bridge pier under study

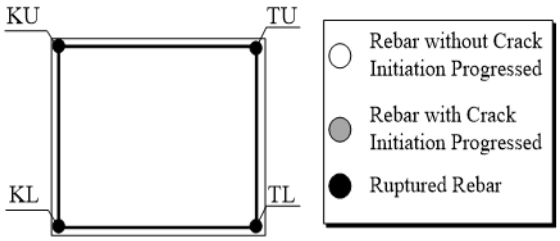

(a) Sectional view and graph legend

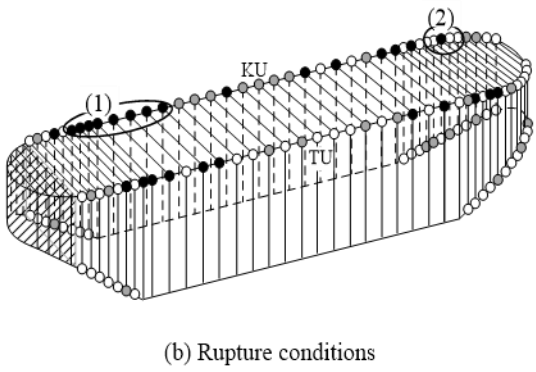

(b) Rupture conditions

Figure 1.3: Rupture of stirrup in the pier under study

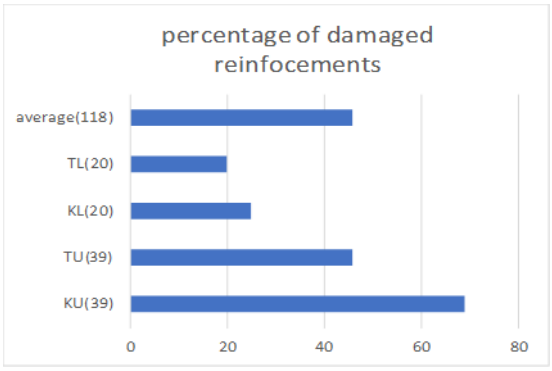

Figure 1.4: Percentage of damaged reinforcements

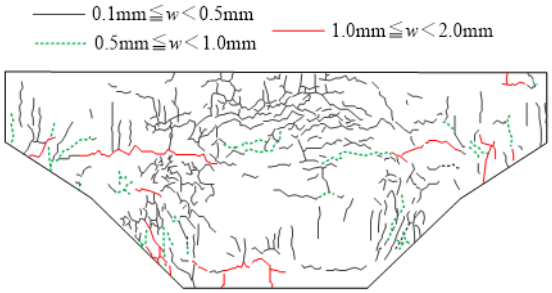

Figure 1.5: Cracking in th profile

Therefore, efforts have been made to identify the rupture mechanism. Based on a JSCE report [3], one of the mainstream estimations is shown in Figure 1.7. First, during the bending process, local strain concentration is produced near the root of ribs, which induces the generation of crack initiation (A of Figure 1.7). Second, considering there is very little plastic deformation and a radial pattern from the crack initiation in the rupture surface [4], angular opening of the corner stirrup was presumed to generate, which led to the progress of crack initiation (B of Figure 1.7). Thus, experiments were conducted for further validation of this estimation.

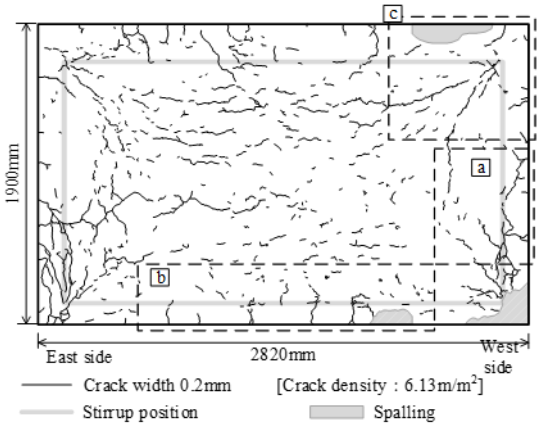

Figure 1.6: Cross-section of the pier beam

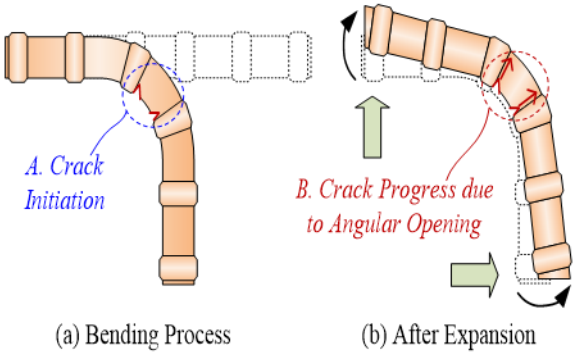

Figure 1.7: Estimated mechanism

2. EXPERIMENTAL INVESTIGATION

In this chapter, the experimental conditions are introduced for a better understanding of the general considerations and basic conditions of the simulation tests.

2.1 Considerations for modelling the specimens

The object for modeling the current specimens is a PC bridge pier beam which has served for over 30 years. The ASR-induced deteriorations and multiple ruptures of stirrups in the bent part were confirmed. As critical failure might occur, a cross-section of 3490 mm×2700 mm near the root of the beam was adopted for modeling. To simulate uniform expansion from ASR, a square cross-section of 680 mm×680 mm nearly 1/4 scale was applied to specimens.

This study examined the effect of ASR-induced inner expansion on damage to external concrete and stirrup fractures. In general, it takes several years for damage by ASR to become evident. To simulate the ASR-induced expansion in the short term, expansive mortar was used. In actual ASR expansion, many factors like creep, dry shrinkage, and anisotropic behavior etc. are very influential [5], [6], [7]. In this study, applying the expansive mortar, the main purpose was set to simply simulate the ASR expansive force itself. The ASR expansive force here can also be imaged as the totally ultimate force which has already considered the integrated influence of factors described above. Based on previous studies [8], [9], the inner expansive force by ASR was considered to be critical on the exterior damage. Thus, a frame of ordinary concrete with 28 days' curing age was arranged in the current specimens, to simply learn about the influence of internal expansive force on the movement and ruptures of corner stirrup.

2.2 Specimen conditions

Using parameters such as different stirrup ratio, reinforcement type or expansion amount (details can be referred in previous study [10]), specimens (Case 11 to 16) of 1/4 of the actual pier beam were made. Brittle rupture crackings were generated [10], which were similar to ASR-influenced structures. In this study, considering the successful reproduction of actual stirrup ruptures, Case 14 and Case 16 with a larger casting area of expansive mortar and different size of frame concrete were used as representative.

Figure 2.1 shows the size and the reinforcement conditions of Case 14 and 16. As to Case 14 (Figure 2.1(a) and (c)), the external size was 680 mm×680 mm×1340 mm with a cross-section of 1/4 to the actual pier beam. Further, the dimension of the expansive mortar was set as 456 mm × 456 mm. Herein, the frame concrete made by ordinary concrete was applied to supply adhesion from concrete to stirrup. Further, minimum length of stirrup (95 mm) is necessary for providing sufficient adhesion based on former research [5]. Thus, considering placing the stirrup and the main reinforcement roughly in the middle of ordinary concrete and using the covering layer as close to the minimum status 40mm of actual structure, the thickness of frame concrete was set to be 112mm. To get the same stirrup ratio of 0.22%

as the actual pier beam with stirrup ruptures, 5 stirrups (D16 rebar) are set up with the spacing of stirrups to be 285 mm and the spacing to concrete surface as 100 mm in each end.

Specimen conditions for Case 16 are illustrated in Figure 2.1(b) and (d). In order to study the influence of different restraints of frame concrete, the dimensions of the cross-section for expansive mortar was the same as 456 mm×456 mm; while the size of frame concrete was 230 mm greater than the 112 mm of Case 14. To make an identical stirrup ratio of 0.22%, 8 stirrups (D16 rebar) are adopted with the spacing of stirrups to be 200 mm and the spacing to concrete surface as 100 mm in each end. As in Figure 2.1(c) and (d), stirrups adopted the D16 reinforcement with one type using a rib shape based on current specifications ('current type' for short) and two types using bamboo joints (ribs aligned in parallel with spacing) based on old specifications ('old type' B and C). More details on reinforcement types can be found in previous research [10].

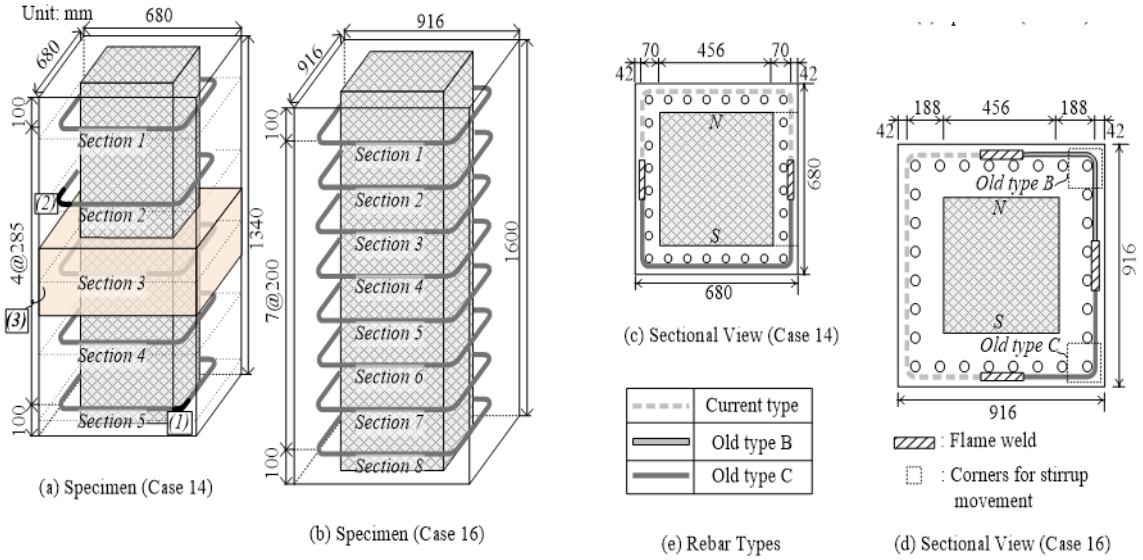

Figure 2.1: Specimens condition

2.3 Material conditions

With respect to material properties, the mix proportions for frame concrete and expansive mortar are presented in Table 2.1 and 2.2, respectively. Frame concrete adopts a strength of 27N/mm^2 as the design strength for the actual pier beam. By cylinder tests after 28 days' curing, the real strength of 35N/mm^2 was obtained. To simulate inner expansion from ASR quickly, a lime-type expansion agent was applied. The expansion agent was set as 200kg/m^3 to reproduce severe deterioration conditions. In addition, in order to imitate strain aging in the bent section of a stirrup, all reinforcements after the bending process were heated under an electric furnace for 10 hours at 120˚C. Consequently, 6 years' progression of strain aging was resulted [11].

Table 2.1: Mix proportions for frame concrete

W/(C+E) (%)	E/(C+E) (%)	Unit (kg/m^3)			
		W	C	S	E
29.8	25.8	231	575	1150	200

Table 2.2: Mix proportions for expansive mortar

G_{max} (mm)	W/C (%)	s/a (%)	Unit (kg/m^3)				
			W	C	S	G	Admixture
20	46	43	175	381	718	1018	1.142

2.4 Measurement items

Here, the measurement items are introduced. To understand the damage behavior of frame concrete and inner stirrups induced by the effect of inner expansion, external cracking, deformation, and damage

produced in inner stirrups were measured for both cases. To evaluate the movement of stirrups directly, the shapes of stirrups were recorded before and after expansion for Case 16. Detailed measurement methods and results are evaluated in subsequent chapters.

3. EVALUATION FOR GENERATION OF CRACKING

The generation mechanism of concrete deformation and cracking was evaluated to understand the casual factors of the deformation condition of the stirrup.

3.1 General cracking conditions

The measurement method for cracking is illustrated in Figure 3.1. Measuring lines with an interval of 100 mm were drawn in a transverse direction to the main reinforcement before expansion. Cracking was measured by crack gauge and sketched at 1.0 hr interval when the development was acute; while a longer time interval was applied in a smaller pace. Measurement objectives were cracking with width greater than 0.05 mm. Further, in order to study the characteristics of cracking in different regions, evaluation areas were divided with a corner area for frame concrete and center area for the other region (refer to Figure 3.1).

Thus, to study the influence from inner expansion on the damage level of concrete, the cracking density and strain were evaluated (definitions in Figure 3.1). Herein, as a boundary width to judge the soundness of structure [12], cracking greater than 0.2 mm was counted for computation of cracking density; cracking strain was defined as the ratio of the sum for cracking width in the measuring line to the length of the measuring line as 680 mm for Case 14 and 916 mm for Case 16 (refer to Figure. 2.1). Thus, the time evolution of cracking strain and density is shown in Figure 3.2. Due to different casting seasons of two cases (Case 14 in winter and Case 16 in summer), the maximum expansion time was 24.0 hr for Case 14, which was greater than 7.75 hr of Case 16 (0 hr as the time point when expansive mortar had just been cast). However, both cases had a similar variation trend as an acute increment at first and the tendency to converge.

For cracking density, the maximum was 7.89m/m^2 for Case 14, which was 2.3 times the 3.39m/m^2 for Case 16. Whereas, for cracking strain, the maximum 8572 μ for Case 14 was 3.1 times the 2789 μ for Case 16. By increasing the size of frame concrete from 112 mm of Case 14 to 230 mm of Case 16, the cracking strain reduced more seriously than cracking density. This suggests that multiple cracking with a small width, which will not be counted in the calculation of cracking density, might occur for Case 16. Referring to research [10], the cracking density and strain of the actual pier beam with ruptures were 2.9 m/m^2 and 2464 μ, respectively. The current two cases show sufficient damage level to induce stirrup rupture. Thus, to check the general cracking form, Figure 3.3 presents the final surface cracking for Cases 14 and 16. Longitudinal cracking was generated in both corners and center areas. Regarding the actual ASR-influential pier beam, cracking was also confirmed to occur in both the center and corner of the profile along with the main reinforcement [13]. Due to the greater restraint from frame concrete, integral cracking widths of Case 16 were on a smaller level, which corresponds to that described in Figure 3.2.

As a result, absolute values of cracking indicators like cracking strain and density were different due to different specimen conditions. However, the general cracking form and the time variation trend in cracking densities and strains were similar to those of the actual structures as a whole.

3.2 Time development of cracking

In order to understand the generation features of cracking and to study the physical impacts from expansion, the time variation of cracking was evaluated. Figure 3.4 shows the record for Case 14 (the south profile for instance, refer to Figure 2.1). Being similar to those described in Figure 3.3, cracking widths were presented by dotted or solid line based on cracking width with the boundary 0.2 mm. After 8.0 hr of expansion, first cracking occurred in the longitudinal direction of the center area. After 10 hr, new cracking appeared in both the corner and the center. Finally, after 24.0 hr, new cracking was slightly produced with the width increasing to 3.0 mm in the center and 8.0 mm in the corner. For contrast, Figure 3.5 shows the evolution of Case 16 (south profile). Similarly, cracking in the greater width occurred in the center first after 2.80 hr. Thus, new cracking appeared in both areas after 3.25 hr. In the final state, almost no new cracking was generated with the maximum width rising to be 1.30 mm and 0.70 mm for the center and the corner, respectively. Similar to findings of previous research [5], two

cases also had variations in cracking arising in the center and then in the corner, while further growth only occurred in width from existing cracking subsequently.

In general, cracking developed in the longitudinal direction due to the smaller restraint of the lateral stirrups. By increasing the size of the frame concrete, the cracking in the profile of Case 16 had a similar form and time variation trend to that of Case 14. Whereas, the general cracking widths of Case 16 were on a smaller level. Figure 3.5 shows that cracking presented in the profile roughly extend to the upper section. In the evaluation of cracking types in order to understand the generation mechanism, cracking in the upper section was examined subsequently.

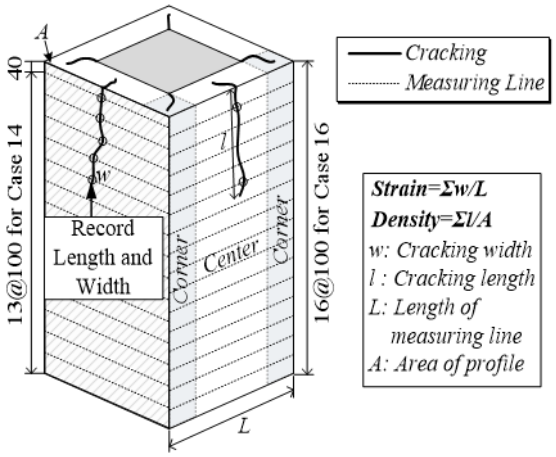

Figure 3.1: Measuring method of cracking

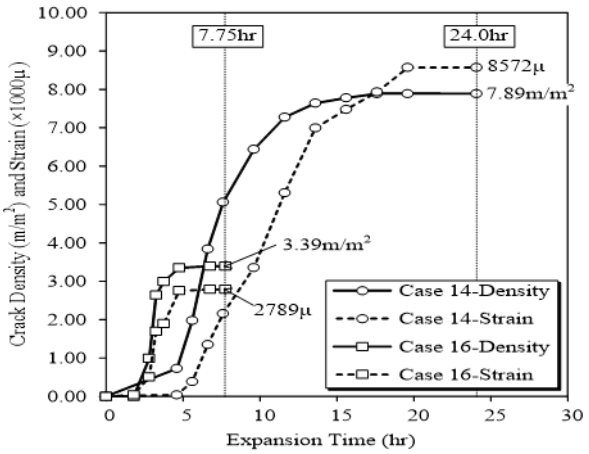

Figure 3.2: Comparison of cracking density and strain

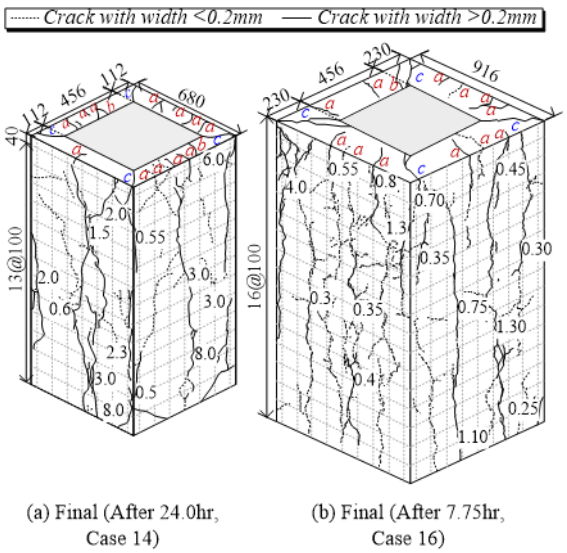

Figure 3.3: General cracking form

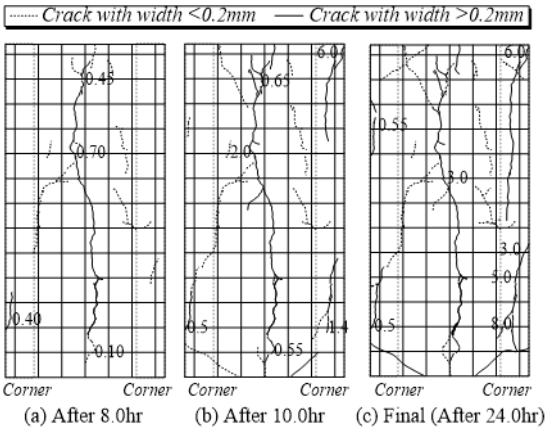

Figure 3.4: Time variation of cracking in surface

3.3 Classification and comparison of cracking types

Cracking types are classified below. Figure 3.6 presents an image of cracking in the upper section together with the possible generating mechanism. As in Figure 3.6(a), due to greater restraint from the concrete and stirrup in the corner area, a positive bending moment will act on the center area of the frame, which induces cracking generated from the exterior (Type a). Simultaneously, due to the rigid constraint in the corner area, negative bending moment will also impact on regions close to corner areas, which causes cracking propagation from the interior (Type b). An image of cracking in the corner part is

shown in Figure 3.6(b). Affected by uniform inner expansion, uniform tension (T) was also generated, which induced cracking to spread throughout in the diagonal direction (Type c).

Consequently, cracking types for Case 14 and Case 16 are illustrated in Figure 3.7(a) and (b), respectively. It was clarified that Type a mainly occupied the center while Type c was the main type in the corner. Further, the numerical statistics for cracking numbers of each type are displayed in Figure 3.7(c). Although with slight variations for cracking numbers, with increasing size of frame concrete in Case 16, no great change was found for cracking type.

As a feature of cracking, by increasing the size of frame concrete, cracking strain and density decreased by over one half. However, the amount for each cracking type did not vary between Cases 14 and 16, which suggested that the cracking form was not influenced by parameters. Further, as the generation mechanism, it was considered that due to the restraint from concrete and stirrup in the corner, inner expansion produced bending effect which induced cracking in the center generated from exterior. Whereas, due to the restraint from both side of frame concrete, the uniform inner expansion also generated tensile effect which induced cracking in the corner to run in the diagonal direction.

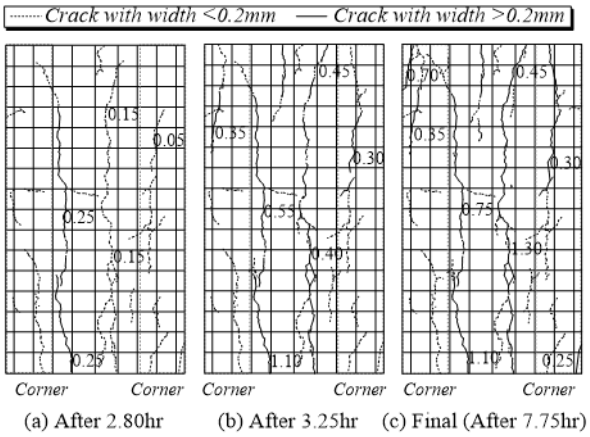

Figure 3.5: Time variation of cracking in surface

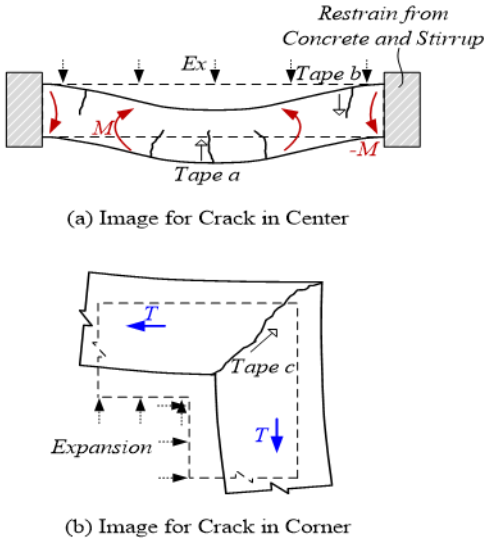

Figure 3.6: Classification for cracking types

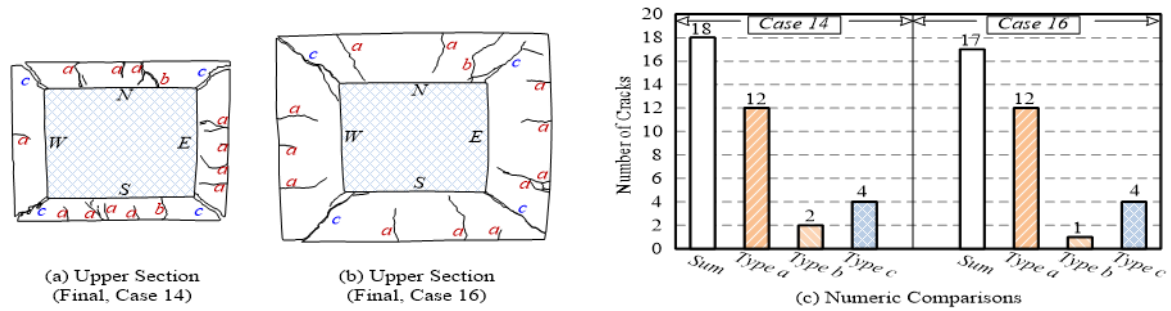

Figure 3.7: Classification of cracking types

4. EVALUATION FOR GENERATION OF DEFORMATION

The features of circumferential deformation as well as its possible influence on stirrup motion were evaluated.

4.1 General deformation conditions

To understand the deformations in cross-sections of stirrups, Figure 4.1 illustrates the measurement method. Cross-sections with the arrangement of five stirrups were the measurement objectives. As shown in Figure 4.1(a), a fixed frame was set around each cross-section. To obtain the length from the fixed frame to the concrete surface, the measuring scale was set at a position 40 mm away from the endpoint of the corner and then followed by each 100 mm (refer to Figure 4.1(b) and (c)). From the calculation of the difference in value of the lengths between fixed frame and concrete surface before and after expansion, the deformation was obtained (e.g., based on the difference of initial length and length after expansion displayed in Figure 4.1 (b) and (c), vertical deformation from Point a_1 to a_2 and from b_1 to b_2 is 3.0 mm and 8.0 mm, respectively). Furthermore, deformation was considered to be composed of two parts as the uniform elongation (uniformly deformed part in the cross-section) and circumferential deformation (roundly deformed part). Thus, deformation a (vertical deformation from a_1 to a_2, Figure 4.1(c)) in the corner point was defined as uniform elongation; while the difference between the maximum deformation b of the cross-section (vertical deformation from b_1 to b_2, Figure 4.1(c)) and the uniform elongation a was defined as circumferential deformation (5.0 mm as the difference between 8.0 and 3.0 mm).

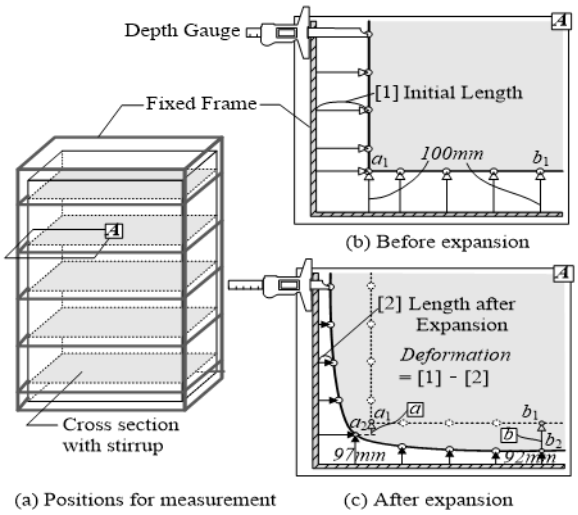

Figure 4.1: Measurement of deformation

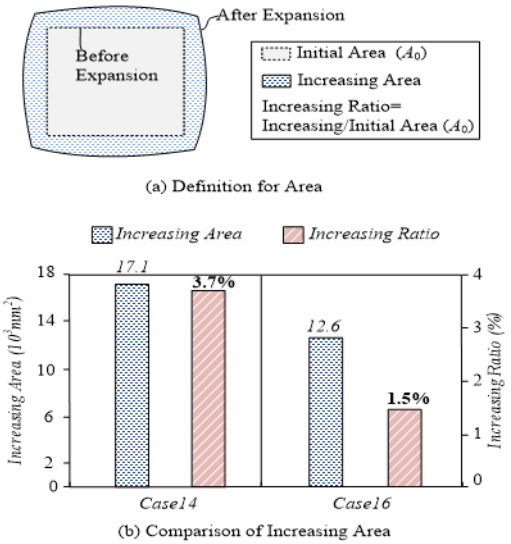

Figure 4.2: Comparison of increasing area of cross-section

Therefore, to understand the general deformation level, the increasing area of the cross-section was evaluated first. As illustrated in Figure 4.2(a), increasing area was defined as the difference between the area after expansion and the initial area (initial area as 464200 mm^2 and 839056 mm^2 for Case 14 and Case 16 (refer to Figure 2.1)). From the results shown in Figure 4.2(b), it was found that Case 14 had an increasing ratio of area of 3.7% to be 2.5 times that of 1.5% for Case 16, induced by smaller restraint of frame concrete.

Subsequently, to understand the general deformation forms, final deformations of Case 14 and 16 are shown in Figure 4.3. The value illustrated is the average deformation in each profile. As for Case 14 (Figure 4.3(a)), deformation increased gradually toward the center area. All cross-sections were confirmed to have circumferential deformation, which was considered to be very influential on the movement of the stirrup [10]. Further, in both ends of the specimen (Cross-sections 1 and 5), the average deformation had greater values than the other cross-sections, which was due to the easier expansion from lesser restraints of stirrups in both ends. On the other hand, for Case 16 (Figure 4.3(b)), as the maximum deformation occurred in the center of the profile, the general circumferential deformation was also confirmed. Similar to the case described above, deformations in both ends of the specimen were of a greater level. However, deformation values were on a smaller level because of greater constraints than Case 14. Accordingly, it was indicated that similar to the growth of cracking, although the absolute values of deformation was different between different cases, a similar deformation form, which is composed of uniform elongation and circumferential deformation, was confirmed.

4.2 Time-dependent variation and classifications

To understand the time-dependent features of deformation, the situations of Case 14 are shown in Figure 4.4. Here, due to the slight variation in deformation form and values between cross-sections 2, 3, and 4 (refer to Figure 4.3(a)), the average deformation in each corresponding point was applied. After 8.0 hr of expansion (Figure 4.4(a)), the values in the profile such as A signified the maximum deformation of each profile; while the values in corners such as B mean deformations in the x and y direction of corner points. Thus, uniform elongation was obtained as 0.50 mm (average of eight values in corners). The average circumferential deformation was 0.84 mm. Together with further expansion after 10.0 hr (Figure 4.4(b)), deformations expanded in general with the maximum in the center of 4.50 mm while that in the corner varied to be 2.33 mm. Finally, for the ultimate state (Figure 4.4(c)), the maximum deformation separately changed to 8.85 and 4.21 mm in the center and the corner.

To understand the variation trend in classified deformations, Figure 4.5 presents the data for each time point. Points (1), (2), and (3) in Figure 4.5 correspond to those in Figure 4.4. As denoted in Figure 4.5(a), uniform elongation increased slowly before 8.0 hr (point (1)). Subsequently, as cracking was confirmed to appear in the profile of the specimen (refer to Figure 3.4(a)), the rigidity of frame concrete was estimated to decrease and thus deformation showed an intense rise from time point (1). After 11.0 hr, the increment of deformation began to decrease. Expansion was supposed to converge after this time point (cracking also had no great variation from 10.0 hr to 24.0 hr (refer to Figure 3.4(b) and (c))). Finally, the maximum uniform elongation was confirmed as 3.33 mm.

Additionally, as shown in Figure 4.5(b), the circumferential deformation had a similar variation trend to uniform elongation. In 24.0 hr (point (3)), circumferential deformation changed to a maximum of 5.00 mm. Specimens using ASR reactive aggregates were also examined by the authors [14]. A similar circumferential deformation near 1.0 mm was also validated to generate after around 1113 days' outdoor exposure. The current specimen using expansive mortar to simulate the inner expansion was considered to have reproduced the ASR-induced circumferential deformation being crucial for stirrup ruptures.

A comparative study for Case 16 was conducted. After 2.80 hr of expansion as in Figure 4.6(a), deformations were produced with maximum 5 mm and 2 mm in the center and the corner, respectively. After 3.25 hr (Figure 4.6(b)), the value in the center increased to a maximum of 6 mm while in the corner it showed no variation. In addition, for the final state (7.75 hr, Figure 4.6(c)), general deformation had a slight increment while maximum values remained the same. For each time point, it was clarified that deformation rose from the corner to the center of the profile. Circumferential deformation such as Case 14 grew over time.

Time evolutions for two types of deformation are illustrated in Figure 4.7. For contrasting variation trends between Case 16 and Case 14 (Figure 4.5), the definition for dimensionless time was applied. The time ratio 1.0 was defined as the end time of expansion to be 7.75 hr for Case 16 and 24.0 hr for Case 14. As denoted in Figure 4.5, deformations increased slowly before 1.80 hr (time ratio 0.2). After that, values had an intense rise before 3.75 hr (ratio about 0.5). Thus, deformations became stable with the maximum value. Additionally, as in Figure 4.5, Case 14 also had a smaller increase before 8.0 hr (time ratio 0.3) and then intense growth until 11.0 hr (time ratio around 0.5) and a slight variation at the end. A similar time variation tendency was verified for two cases.

To investigate the reason for this development tendency, the inner temperature measured from Case 16 was evaluated. As shown in Figure 4.8, before expansion, a recording thermometer was input in the central point of the cross-section, which was located at 800 mm from the upper side (central section). Therefore, from the recorded results, it was found that temperature increased dramatically from the initial value of around 37˚C up to 3.75 hr (time ratio 0.5) for the maximum at 106˚C. After that, values began to decrease due to convergence of the reaction.

Thus, in contrast to the deformation progress illustrated in Figure 4.7, the great rise of inner temperature corresponded to the intense increase of deformation (Stage B) before 3.75 hr (time ratio 0.5). After that, the decrease of temperature caused reduction of the reaction speed for expansion and thus slowed the development pace of deformation.

4.3 Image for the generating mechanism

The image for the generation mechanism and its possible connection to stirrup motion are discussed. Distributed load was assumed to act on the frame concrete. The frame part AB (Figure 4.9(a)) was the center line and assumed to receive fixed restraint in both ends. Thus, due to the restraint in the corner

part, the distributed load in the vertical direction w_y produced moment (M) with the distribution imaged in Figure 4.9(b). Corresponding maximum deformation δ_m was then generated in the central frame. Further, the distributed load in horizontal direction w_x transmitted to part AB and resulted in axial force (N) with uniform distribution as referred to in Figure 4.9(b). Similarly, deformation δ_n was yielded. Therefore, it was considered that the circumferential and uniform elongation correlated with δ_m and δ_n, which were generated from the bending and tensile effects, respectively. Moreover, due to greater restraint in the corner from the greater size of frame concrete for Case 16, it was noted that the ratio of circumferential to uniform elongation was 2.6 (refer to Figure 4.7), being greater than the 1.5 of Case 14 (Figure 4.5). Thus, greater external restraint was found to induce a larger proportion of circumferential deformation.

Therefore, greater external restraint caused a greater proportion of circumferential deformation. Further, as an integral summary of former chapters, it was considered that restraint in the corner induced a bending effect, which promoted cracking in the center generating from the exterior. Correspondingly, circumferential deformation was produced. Besides, as in Figure 4.9(c), for possible influence on stirrup motion, general circumferential deformation might be influential on the angular opening of corner stirrup.

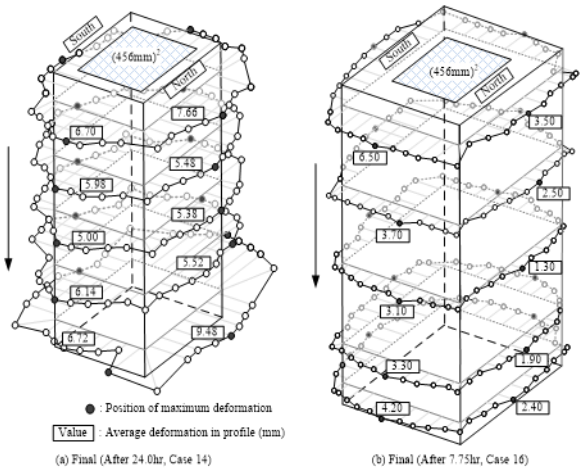

Figure 4.3: General deformation forms

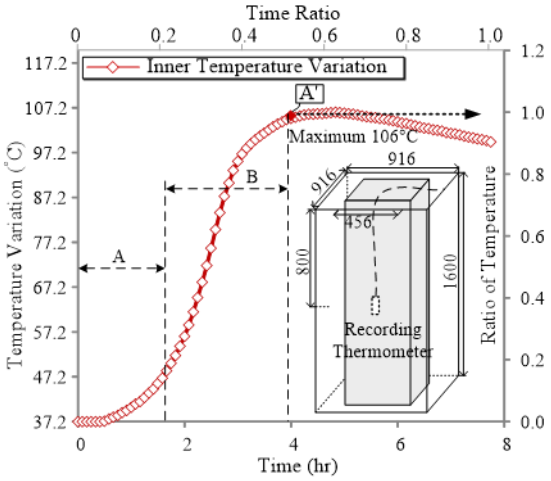

Figure 4.8: Time variation of inner temperature (Case16)

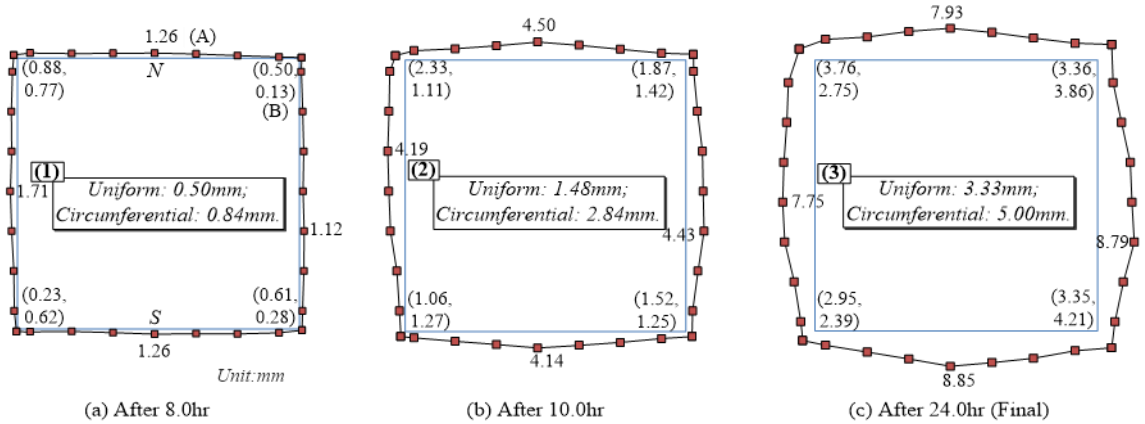

Figure 4.4: Time variation for general deformations (Case 14)

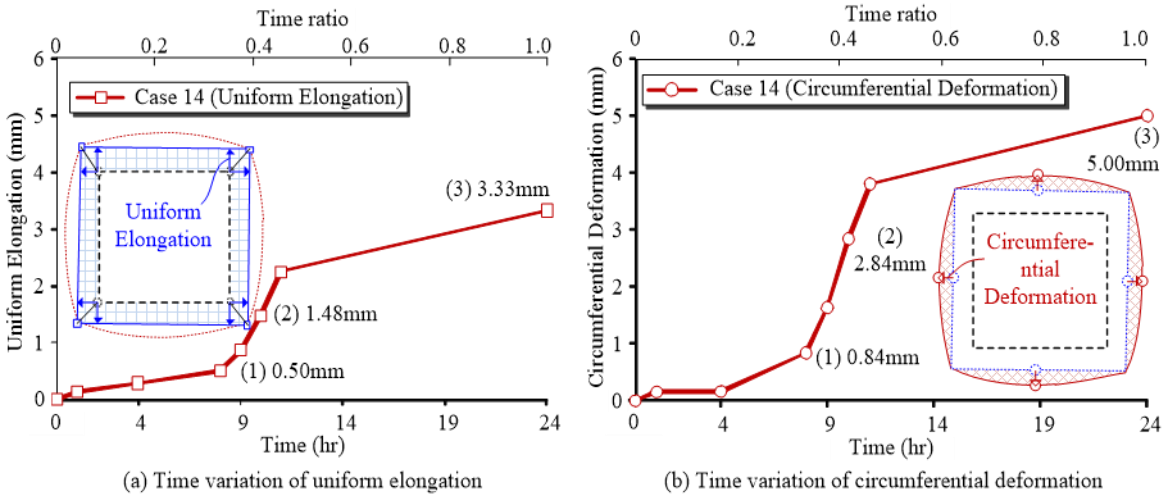

(a) Time variation of uniform elongation (b) Time variation of circumferential deformation

Figure 4.5: Time variation of classified deformation

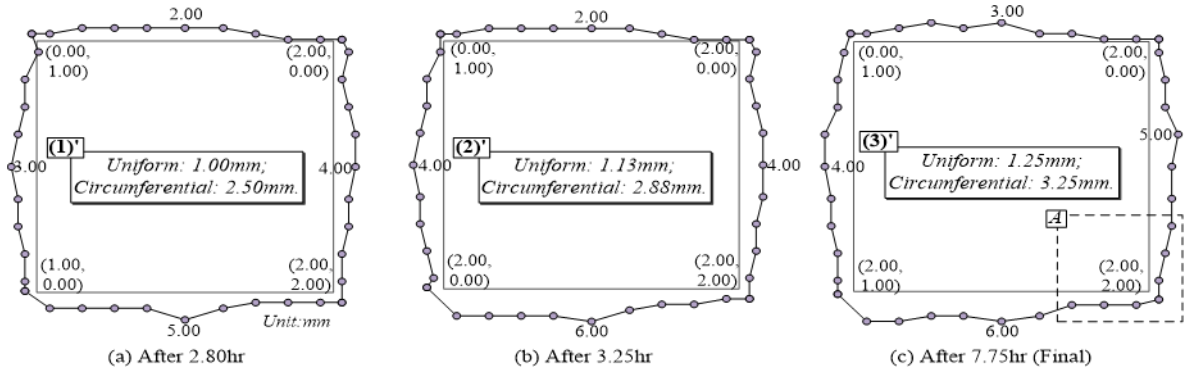

(a) After 2.80hr (b) After 3.25hr (c) After 7.75hr (Final)

Figure 4.6: Time variation for general deformations(Case16)

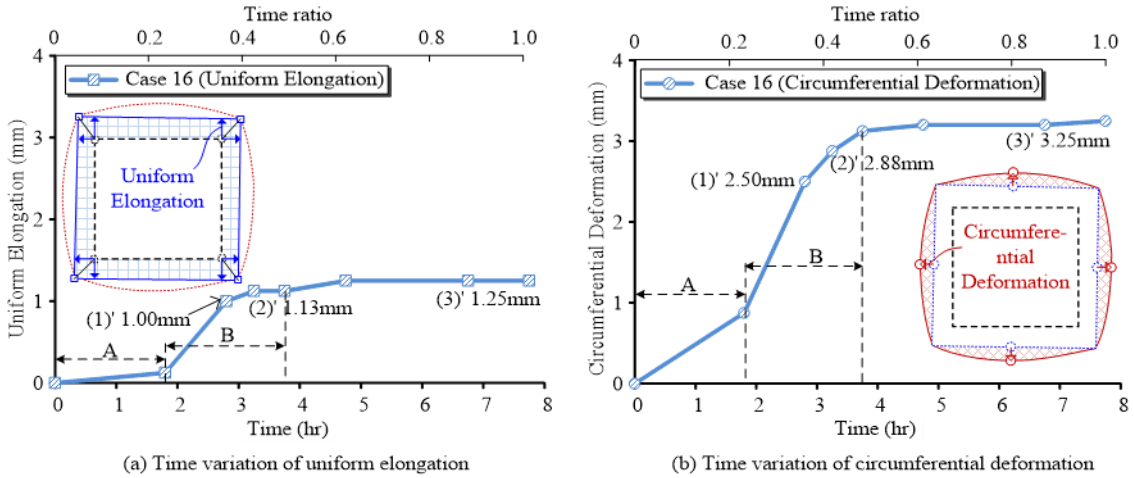

(a) Time variation of uniform elongation (b) Time variation of circumferential deformation

Figure 4.7: Time variation for classified deformation

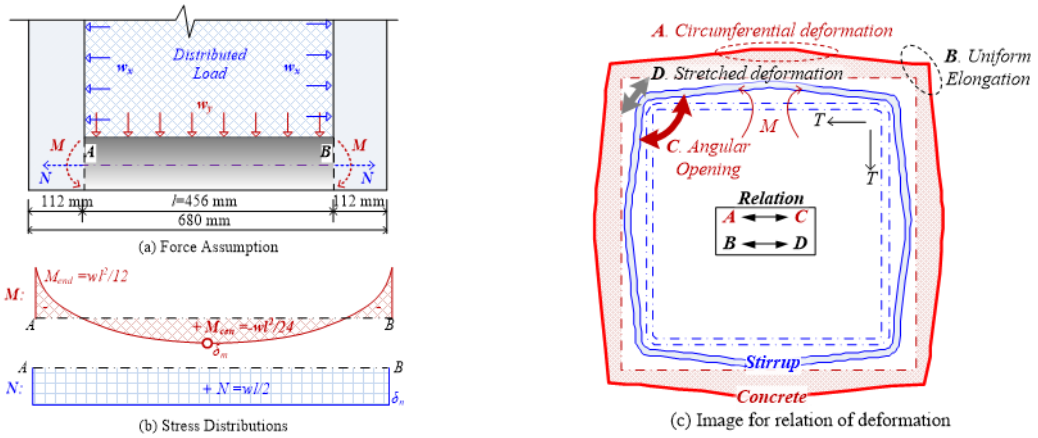

Figure 4.9: Mechanism for generation of deformation

5. CONCLUSIONS

To estimate stirrup behavior, which is very influential on a rupture around a stirrup due to ASR, specimens with expansive mortar cast into the frame of ordinary concrete were investigated. The mechanism for external damage and its influence on the stirrup motion and further on the progress of crack initiation was studied to confirm the rupture mechanism. The following conclusions were obtained:

1)Cracking conditions were evaluated to discuss the effects of ASR-inner expansion. By increasing the size of frame concrete from 112 mm of Case 14 to 230 mm of Case 16, greater restraint caused both cracking density and cracking strain seriously decreased to be 3.39m/m^2 and 2789 μ, respectively. While, the current two cases show sufficient damage level to induce stirrup rupture as the cracking density and strain of a pier beam with ruptures were 2.9m/m^2 and 2464 μ.

2)Cracking in external concrete were divided into three types: Type a for cracking occurred from the exterior and this is estimated to be caused by the positive bending effect in the center area; Type b for cracking generated from the interior, which is considered to be caused by the negative bending effect near the corner; and, Type c for cracking spreading throughout the diagonal direction and this is thought to be the effect from the uniform tension in the corner. For both cases, it was clarified that Type a mainly occupied the center (amount as 12 in total 18 for Case 14 and 12 in total 17 for Case 16) while Type c was the main type in the corner (amount as 4 in total 18 for Case 14 and 4 in total 17 for Case 16), which suggests that the cracking form is not influenced by parameters.

3)Corresponding to cracking, external deformation conditions were evaluated. With increment for size of frame concrete, restrain raised which induced the increasing ratio of deformation area varied from 3.7% of Case 14 to 1.5% of Case 16. Deformation was classified as uniform elongation (uniformly deformed part in the cross-section) and circumferential deformation (roundly deformed part). By increasing the size of the frame concrete, the ratio of circumferential deformation to uniform elongation raised from 1.5 to 2.6. Greater external restraint causes a greater proportion of circumferential deformation.

4)As a result, it was presumed that due to the restraint from concrete and stirrup in the corner, inner expansion produced bending effect, which produced the circumferential deformation in general profile together with the notable cracking in the central part of profile in structure to occur.

6. REFERENCES

[1] Torii, K. (2010) The Characteristic Feature of Fracture of Steel Reinforcement in ASR-Deteriorated Concrete Structures, Zairyo-to-Kankyo, Vol. 59 Issue 4, 117-120.

[2] Uehara, N. (2016) Rebar Damage and Internal Degradation of Concrete due to Alkali-Aggregate Reaction, Doctoral Thesis, 22-46.

[3] JSCE (2005) State-of-the-Art Report on the Countermeasures for the Damage Due to Alkali-Silica Reaction, Concrete Library, No. 124, 1-32~1-65.

[4] Sasaki, K., Fujibayashi, M., Tona, M., Sato, A., Hisari, Y. and Miyagawa, T. (2013) Investigation of the cause of reinforcing steel fracture induced by alkali-silica reaction and study on maintenance, Third International Conference on Sustainable Construction Materials and Technologies.

[5] Kosa, K., Kawashima, Y., Goda, H. and Kouroki, N. (2008) Experimental tests on breaking mechanism of reinforcing bars subjected to alkali silica reaction, Journal of JSCE, Ser. E, Vol. 64, No. 2, 371-388.

[6] Mielich, O., Ozkan, H. and Reinhardt, H. W. (2016) Creep behavior of alkali-silica reaction damaged concrete with slow-reacting aggregates, 15th International Conference on Alkali Aggregate Reaction in Concrete, Sao Paulo.

[7] Giorla, A., Dunant, C., Guidoum, A. and Scrivener, K. (2016) Experimental and numerical study of alkali-silica reaction under multi-axial load, 15th International Conference on Alkali Aggregate Reaction in Concrete, Sao Paulo.

[8] Kobayashi, K., Shiraki, R. and Kawai, K. (1988) Expansion and cracking of concrete structures caused by alkali silica reaction, Seisan Kenkyu, Vol. 40, No. 12, 616-619.

[9] Kagimoto, H., Yasuda, Y., Kinoshita, S. and Kawamura, M. (2014) Mechanisms of ASR surface cracking in a massive concrete cylinder, Concrete Research and Technology, Vol. 25, 201-211.

[10] Kosa, K., Kusano, M., Goda, H. and Shibata, A. (2013) Evaluation of deterioration using an ASR-imitated test specimen, Journal of JSCE, Ser. E2, Vol. 69, No. 2, 166-181.

[11] Hundy, B. B. (1954) Accelerated strain ageing of mild steel, Journal of the Iron Steel Institute, 34-38.

[12] Hanshin Expressway Public Corporation (1985) Standard for Maintenance Inspection of Road-structures (Civil Engineering Structure Part).

[13] Kusano, M., Kosa, K., Goda, H. and Masuda, H. (2010) Large specimen test conducted to evaluate the progress of cracking of reinforcing bars due to ASR, Journal of Structural Engineering. A, Vol. 56A, 891-900.

[14] Kusano, M., Kosa, K., Akiyoshi, S. and Goda, H. (2011) Evaluation for progress of stirrup damages using ASR specimens, Proceedings of the Japan Concrete Institute, Vol. 33, No. 1, 989-994.